

Synthesis and Dielectric Properties of Complex Perovskite oxides obtained from Perovskite Nanosheets

Keigo Inaba*, Shinya Suzuki*, Yuji Noguchi*, Masaru Miyayama*, Minoru Osada**

*RCAST, The University of Tokyo, 4-6-1 Komaba, Meguro-ku, Tokyo

Fax: 03-5452-5081, e-mail: kinaba@crm.rcast.u-tokyo.ac.jp

**Advanced Materials Laboratory, National Institute for Materials Science, Tsukuba, Ibaraki 305-0044, Japan

We synthesized the perovskite-type oxides with A-site vacancies, $\text{Sr}_{0.5}\text{NbO}_3$, $\text{Sr}_{0.5}\text{TaO}_3$ and $\text{Sr}_{0.5}\text{Nb}_{0.5}\text{Ta}_{0.5}\text{O}_3$, via nanosheet process using $(\text{SrNb}_2\text{O}_7)^{2-}$ nanosheets and/or $(\text{Sr}_{1.5}\text{Ta}_3\text{O}_{10})^{2-}$ nanosheets. Raman scattering demonstrates that nanosheet-processed $\text{Sr}_{0.5}\text{Nb}_{0.5}\text{Ta}_{0.5}\text{O}_3$ have a novel structure composed of the alternate stacking of the several layers of $\text{Sr}_{0.5}\text{NbO}_3$ and $\text{Sr}_{0.5}\text{TaO}_3$ along the c axis. Dielectric measurements (1 MHz) of pressed powder exhibited that nanosheet-processed $\text{Sr}_{0.5}\text{TaO}_3$ showed a much higher permittivity of 52 compared with solid-state-reacted $\text{Sr}_{0.5}\text{TaO}_3$ (33). Nanosheet-processed $\text{Sr}_{0.5}\text{Nb}_{0.5}\text{Ta}_{0.5}\text{O}_3$ with B-site-cation ordering had a lower permittivity of 42 than that with B-site-cation disordering (65). These results suggest that the stacking faults induced by nanosheet process and the arrangement of B-site cations play an important role in dielectric permittivity.

Key words: Nanosheets, Reassembled Materials, Complex Perovskite Oxides, Dielectric Permittivity

1. INTRODUCTION

Perovskite oxides with a layered structure exhibit large amounts of useful properties, including ion exchanging¹⁾, intercalation²⁾, catalysts³⁾ and superconductors⁴⁾. Layered-perovskite oxides are classified into the Ruddlesden-Popper (RP) type oxides $\text{A}'_2[\text{A}_{m-1}\text{B}_m\text{O}_{3m+1}]^{5)}$, the Dion-Jacobson (DJ) type oxides $\text{A}'[\text{A}_{m-1}\text{B}_m\text{O}_{3m+1}]^{6)}$ and the Aurivillius type oxides $(\text{Bi}_2\text{O}_2)[\text{A}_{m-1}\text{B}_m\text{O}_{3m+1}]^{7)}$, where A' represents alkali metals; A represents La^{3+} , Pb^{2+} , Sr^{2+} etc. at the 12-coordinated site; B represents Ti^{4+} , Nb^{5+} , Ta^{5+} etc. at the 6-coordinated site; and m is an integer number of BO_6 octahedra.

The alkali metal A' can be easily exchanged with H^+ or H_3O^+ in acid solution to form protonated RP-type oxides $\text{H}_2[\text{A}_{m-1}\text{B}_m\text{O}_{3m+1}]^{8)}$ and DJ type oxides $\text{H}[\text{A}_{m-1}\text{B}_m\text{O}_{3m+1}]^{9)}$. Protons in these layered-perovskites play an important role in the reactions of dehydration¹⁰⁾, intercalation¹¹⁾ and exfoliation¹²⁾. For example, the dehydration of $\text{H}[\text{A}_{m-1}\text{B}_m\text{O}_{3m+1}]$ with 2-dimensional (2D) layered structure results in 3-dimensional (3D) perovskite $\text{A}_{m-1}\text{B}_m\text{O}_{3m+1}$ (metastable) with a cation deficiency at the A site. Additionally, the intercalation of larger ions into $\text{H}[\text{A}_{m-1}\text{B}_m\text{O}_{3m+1}]$ expand the distance between the perovskite layers of $\text{A}_{m-1}\text{B}_m\text{O}_{3m+1}$, and then extremely thin layers composed of $\text{A}_{m-1}\text{B}_m\text{O}_{3m+1}$ has been successfully obtained by exfoliation¹²⁻¹⁶⁾.

Recently, thin plate-like oxide with a thickness of a few nanometer, i.e., nanosheets, composed of several $\text{A}_{m-1}\text{B}_m\text{O}_{3m+1}$ layers obtained from the exfoliation of protonated RP type oxides

and DJ type oxides have been studied as novel nanostructured materials¹²⁻¹⁶⁾. These nanosheets have unique characteristics such as an extremely high aspect ratio (thickness in a nanometer range) and colloidal nature in aqueous solutions due to their negatively charged surface. The colloidal nanosheets can be reassembled by the chemical reaction with cations such as Na^+ and $\text{K}^{+14)}$ in the solutions as a result of electrostatic interaction between them. The reassembled materials can be obtained by stacking the nanosheets interleaved with these cations along the c axis. This process leads to the reassembled material, which has a different stacking structure from the original protonated oxides. Therefore, these nanosheets are expected to be a building block to provide novel nanostructured materials that could not be obtained through traditional methods.

In this study, we synthesized, via the nanosheet process, A-cation-deficient perovskite oxides $\text{A}_{0.5}\text{BO}_3$ and complex perovskite oxides $\text{A}_{0.5}(\text{B}_{0.5}\text{B}'_{0.5})\text{O}_3$ ($\text{A} = \text{Sr}$; $\text{B}, \text{B}' = \text{Nb}, \text{Ta}$). The reassembled $\text{Sr}_{0.5}(\text{Nb}_{0.5}\text{Ta}_{0.5})\text{O}_3$ obtained has a novel stacking structure with alternating Nb and Ta layers along the c axis. Figure 1 shows the schematic representation of the nanosheet process employed in our study. The nanosheet process enables us to obtain a novel perovskite oxide composed of the layers of $\text{A}_{0.5}\text{BO}_3$ and $\text{A}_{0.5}\text{B}'\text{O}_3$ along the c axis. The final goal of this work is to provide dielectric materials with tailored dielectric properties for next-generation multi-layered ceramic capacitors.

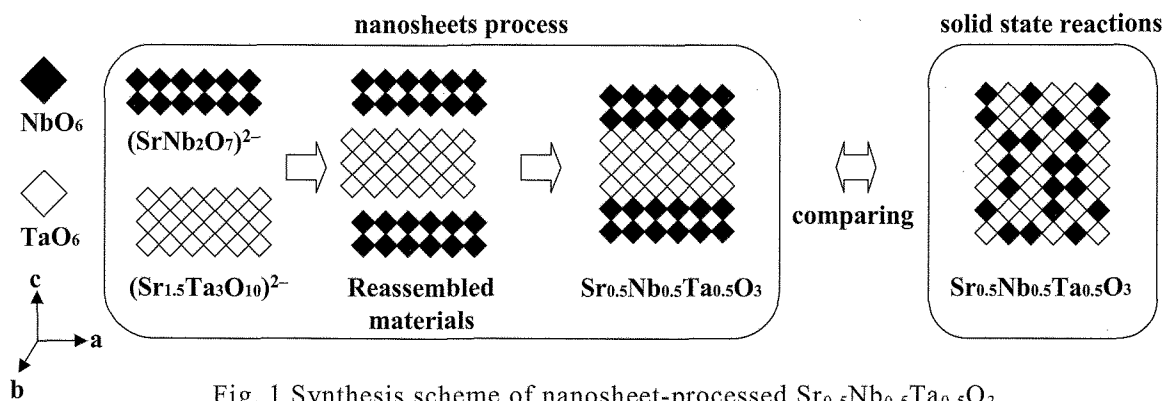


Fig. 1 Synthesis scheme of nanosheet-processed $\text{Sr}_{0.5}\text{Nb}_{0.5}\text{Ta}_{0.5}\text{O}_3$

2. EXPERIMENTAL

RP type oxides $\text{Li}_2\text{SrNb}_2\text{O}_7$ and $\text{K}_2\text{Sr}_{1.5}\text{Ta}_3\text{O}_{10}$ were synthesized according to the literatures^{12, 17}. $\text{Li}_2\text{SrNb}_2\text{O}_7$ were prepared by solid state reaction of stoichiometric amounts of SrCO_3 , Nb_2O_5 and a 40 % molar excess of Li_2CO_3 by sintering at 1100 °C for 3 days with intermediate grindings. $\text{K}_2\text{Sr}_{1.5}\text{Ta}_3\text{O}_{10}$ were synthesized by solid state reactions of stoichiometric amounts of SrCO_3 , Ta_2O_5 and a 40 % molar excess of K_2CO_3 by calcining at 850 °C for 6 h followed by sintering 1200 °C for 10 h. SrCO_3 and K_2CO_3 was pre-dried at 120 °C for 1 day before use. RP-type oxides $\text{K}_2\text{SrNbTaO}_7$ were prepared in a similar manner according to Ref 18. Stoichiometric quantities of SrCO_3 , Nb_2O_5 , Ta_2O_5 and 150 % molar excess of K_2CO_3 were ground and pressed uniaxially into pellets at 7 MPa. The pellets were heated at 850 °C for 1 h followed by sintered at 1050 °C for 12 h. After the first heating cycle, the reactants were again heated at 850 °C for 1 h and subsequently heated at 1150 °C for 12 h. The resultant samples of $\text{Li}_2\text{SrNb}_2\text{O}_7$, $\text{K}_2\text{Sr}_{1.5}\text{Ta}_3\text{O}_{10}$ and $\text{K}_2\text{SrNbTaO}_7$ were washed with water and dried at 80 °C for 1 day. $\text{H}_2\text{SrNb}_2\text{O}_7$ was prepared by ion-exchanging $\text{Li}_2\text{SrNb}_2\text{O}_7$ in 1 M HNO_3 for 5 days at room temperature. The acid was replaced every day with a fresh one to ensure the exchange reaction. $\text{H}_2\text{Sr}_{1.5}\text{Ta}_3\text{O}_{10}$ was prepared from $\text{K}_2\text{Sr}_{1.5}\text{Ta}_3\text{O}_{10}$ in 2 M HNO_3 for 1 day at 60 °C. $\text{H}_2\text{SrNbTaO}_7$ was obtained by titrating the stirred suspension with 0.5 M HCl from a pH of 14 to 6.5.

Exfoliations of $\text{H}_2\text{SrNb}_2\text{O}_7$ and $\text{H}_2\text{Sr}_{1.5}\text{Ta}_3\text{O}_{10}$ are typically achieved by the reactions with a 1-fold-molar-excess tetrabutylammonium hydroxide (TBA^+OH^-) in 300 ml water at room temperature for 3 weeks. The nanosheets of $(\text{SrNb}_2\text{O}_7)^{2-}$ and $(\text{Sr}_{1.5}\text{Ta}_3\text{O}_{10})^{2-}$ were mixed with a ratio of 3:2 and reassembled with 1 M HCl .

The reassembled mixture was topochemically dehydrated by a heat treatment at 500 °C for 2 h. Dehydration process led to nanosheet-processed (NP) $\text{Sr}_{0.5}\text{Nb}_{0.5}\text{Ta}_{0.5}\text{O}_3$ with 3D perovskite structure having A-cation vacancies. NP- $\text{Sr}_{0.5}\text{NbO}_3$ and NP- $\text{Sr}_{0.5}\text{TaO}_3$ were obtained from dehydration of reassembled $\text{H}_2\text{SrNb}_2\text{O}_7$ (2 h at 470 °C) and $\text{H}_2\text{Sr}_{1.5}\text{Ta}_3\text{O}_{10}$ (2 h at 700 °C),

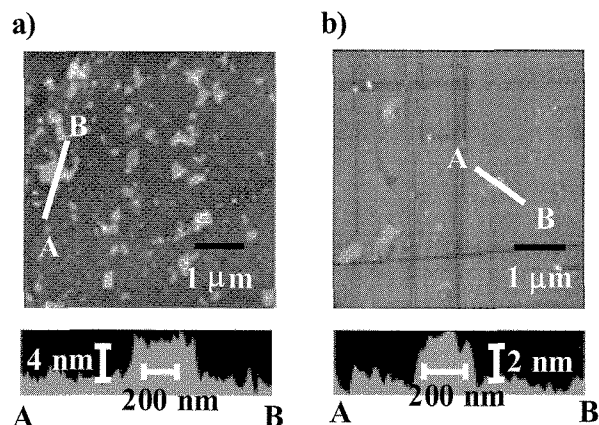


Fig. 2 AFM images of a) $(\text{SrNb}_2\text{O}_7)^{2-}$ and b) $(\text{Sr}_{1.5}\text{Ta}_3\text{O}_{10})^{2-}$ nanosheets

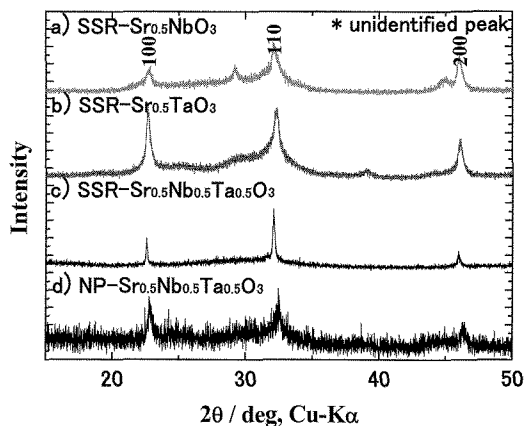


Fig. 3 XRD patterns of SSR- a) $\text{Sr}_{0.5}\text{NbO}_3$, b) $\text{Sr}_{0.5}\text{TaO}_3$, c) $\text{Sr}_{0.5}\text{Nb}_{0.5}\text{Ta}_{0.5}\text{O}_3$ and NP- d) $\text{Sr}_{0.5}\text{Nb}_{0.5}\text{Ta}_{0.5}\text{O}_3$

respectively. Solid-state-reacted (SSR) samples of $\text{Sr}_{0.5}\text{Nb}_{0.5}\text{Ta}_{0.5}\text{O}_3$, $\text{Sr}_{0.5}\text{NbO}_3$ and $\text{Sr}_{0.5}\text{TaO}_3$ were also synthesized by heating $\text{H}_2\text{SrNbTaO}_3$ (2 h at 500 °C), $\text{H}_2\text{SrNb}_2\text{O}_7$ (2 h at 470 °C) and $\text{H}_2\text{SrTa}_2\text{O}_7$ (2 h at 700 °C), respectively.

AFM observations were carried out in a tapping mode. Adsorbed $(\text{SrNb}_2\text{O}_7)^{2-}$ and

$(\text{Sr}_{1.5}\text{Ta}_3\text{O}_{10})^{2-}$ nanosheets on the Quartz glass plates coated with a layer of polyethylenimine (PEI) were subjected for AFM measurements¹⁹. Powder X-ray diffraction (XRD) patterns were obtained using $\text{CuK}\alpha$ ($\lambda=0.15418$ nm) radiation. Raman measurements were performed in a backward micro-configuration, using the 514.5 nm line from an Ar^+ laser (~ 1 mW) focused to ~ 1 μm -diameter spot on the sample surface. The scattered light was dispersed by a subtractive triple spectrometer (HORIBA-Jobin Yvon T64000) and collected with a liquid-nitrogen-cooled charge-coupled device (CCD) detector. For dielectric measurements, the powders were pressed into pellets, annealed for 2 h at 700 °C and then Au electrodes were sputtered onto the both surfaces.

3. RESULTS AND DISCUSSION

Figure 2 shows an AFM image of $(\text{SrNb}_2\text{O}_7)^{2-}$ and $(\text{Sr}_{1.5}\text{Ta}_3\text{O}_{10})^{2-}$ nanosheets. The lower panel depicts a height profile for the cross section along the line "AB" indicated in the upper panel. The thicknesses of $(\text{SrNb}_2\text{O}_7)^{2-}$ and $(\text{Sr}_{1.5}\text{Ta}_3\text{O}_{10})^{2-}$ nanosheets were estimated to be 6 nm and 4 nm, respectively, while the lateral size of both nanosheets was approximately 300 nm. *Ab initio* calculations reveals that the thickness of one perovskite layer of $\text{H}_2\text{SrNb}_2\text{O}_7$ ($m = 2$) is about 0.8 nm. The thickness of the perovskite layer of $\text{H}_2\text{Sr}_{1.5}\text{Ta}_3\text{O}_{10}$ ($m = 3$) calculated from that of $\text{H}_2\text{SrNb}_2\text{O}_7$ ($m = 2$) was about 1.2 nm. These results show that the $(\text{SrNb}_2\text{O}_7)^{2-}$ and $(\text{Sr}_{1.5}\text{Ta}_3\text{O}_{10})^{2-}$ nanosheets in the AFM observations are composed approximately of 7 unit layers and 3 unit layers, respectively²⁰.

Figure 3 shows the XRD patterns of SSR-samples of (a) $\text{Sr}_{0.5}\text{NbO}_3$, (b) $\text{Sr}_{0.5}\text{TaO}_3$, (c) $\text{Sr}_{0.5}\text{Nb}_{0.5}\text{Ta}_{0.5}\text{O}_3$ and (d) NP- $\text{Sr}_{0.5}\text{Nb}_{0.5}\text{Ta}_{0.5}\text{O}_3$. XRD profiles of NP- $\text{Sr}_{0.5}\text{Nb}_{0.5}\text{Ta}_{0.5}\text{O}_3$ are similar to those of SSR-compounds. Broadening of the XRD peaks appeared for NP-samples due to a poor crystallinity caused by low-temperature chemical reaction. The lattice parameter of the NP- $\text{Sr}_{0.5}\text{Nb}_{0.5}\text{Ta}_{0.5}\text{O}_3$ was $a = 0.391$ nm, while those of SSR-samples of $\text{Sr}_{0.5}\text{NbO}_3$, $\text{Sr}_{0.5}\text{TaO}_3$ and $\text{Sr}_{0.5}\text{Nb}_{0.5}\text{Ta}_{0.5}\text{O}_3$ were $a = 0.393$ nm, 0.392 nm and 0.386 nm, respectively. The parameter a of the SSR- $\text{Sr}_{0.5}\text{Nb}_{0.5}\text{Ta}_{0.5}\text{O}_3$ was smaller than that of NP- $\text{Sr}_{0.5}\text{Nb}_{0.5}\text{Ta}_{0.5}\text{O}_3$. The random distribution of B-site cations results in a smaller lattice parameter due to closed packing of the constituent ions, as observed for SSR- $\text{Sr}_{0.5}\text{Nb}_{0.5}\text{Ta}_{0.5}\text{O}_3$. The larger lattice parameter for NP-samples is likely to originate from the superlattice-like structure as depicted in Fig. 1.

Measurements of the Raman spectra were conducted to investigate the local structure in the samples. The spectrum of NP- $\text{Sr}_{0.5}\text{Nb}_{0.5}\text{Ta}_{0.5}\text{O}_3$ was similar to those of SSR samples of $\text{Sr}_{0.5}\text{NbO}_3$ and $\text{Sr}_{0.5}\text{TaO}_3$. These three samples exhibited a peak at around 600 cm^{-1} attributed to A_1 mode, while SSR- $\text{Sr}_{0.5}\text{Nb}_{0.5}\text{Ta}_{0.5}\text{O}_3$ had a peak at about

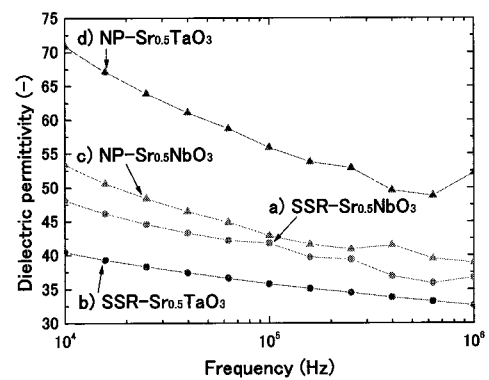


Fig. 4 Dielectric permittivity of SSR- a) $\text{Sr}_{0.5}\text{NbO}_3$ and b) $\text{Sr}_{0.5}\text{TaO}_3$ and NP- c) $\text{Sr}_{0.5}\text{NbO}_3$ and d) $\text{Sr}_{0.5}\text{TaO}_3$

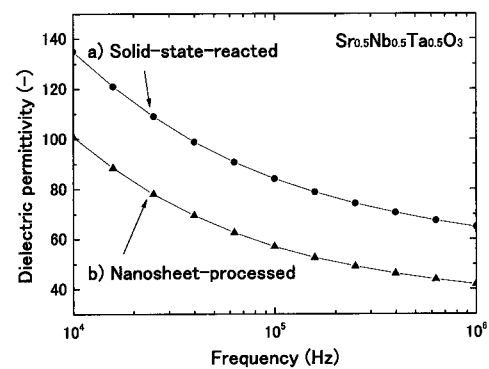


Fig. 5 Dielectric permittivity of a) SSR- and b) NP- $\text{Sr}_{0.5}\text{Nb}_{0.5}\text{Ta}_{0.5}\text{O}_3$

650 cm^{-1} . This difference in peak frequency seems to be attributed to the potential depth of Ti in the TiO_6 octahedra. SSR- $\text{Sr}_{0.5}\text{Nb}_{0.5}\text{Ta}_{0.5}\text{O}_3$ had a smaller lattice parameter a due to a random distribution of Ta and Nb at the B site compared with nanosheet-processed one, and the smaller lattice results in a higher frequency of A_1 mode. These results of the Raman spectra suggest that the local structure of NP- $\text{Sr}_{0.5}\text{Nb}_{0.5}\text{Ta}_{0.5}\text{O}_3$ is similar to SSR-samples ($\text{Sr}_{0.5}\text{NbO}_3$ and $\text{Sr}_{0.5}\text{TaO}_3$) and that $\text{Sr}_{0.5}\text{Nb}_{0.5}\text{Ta}_{0.5}\text{O}_3$ has the superlattice-like structure composed of $\text{Sr}_{0.5}\text{NbO}_3$ and $\text{Sr}_{0.5}\text{TaO}_3$ (see Fig. 1)

Figure 4 showed the dielectric permittivity (ϵ) as a function of frequency of applied oscillation voltage for the SSR- and NP-samples. NP- $\text{Sr}_{0.5}\text{TaO}_3$ exhibited a higher ϵ of 52 than SSR- $\text{Sr}_{0.5}\text{TaO}_3$ (33). ϵ of NP- $\text{Sr}_{0.5}\text{NbO}_3$ was slightly higher than that of SSR- $\text{Sr}_{0.5}\text{NbO}_3$ in the whole frequency range. These results suggest that the stacking faults induced by nanosheets process play an important role in higher ϵ for

NP-samples.

Figure 5 shows ϵ as a function of oscillation frequency for $\text{Sr}_{0.5}\text{Nb}_{0.5}\text{Ta}_{0.5}\text{O}_3$. NP- $\text{Sr}_{0.5}\text{Nb}_{0.5}\text{Ta}_{0.5}\text{O}_3$ with B-site-cation ordering showed ϵ of 42 at 1 MHz, which was higher than that of SSR-samples of $\text{Sr}_{0.5}\text{NbO}_3$ (37) and $\text{Sr}_{0.5}\text{TaO}_3$ (33). In contrast, ϵ of 42 for NP- $\text{Sr}_{0.5}\text{Nb}_{0.5}\text{Ta}_{0.5}\text{O}_3$ was lower than that of SSR- $\text{Sr}_{0.5}\text{Nb}_{0.5}\text{Ta}_{0.5}\text{O}_3$ with the disordering of the B-site cations (65). These results indicate that the arrangement of B-site cations affects the dielectric property of the complex-perovskite system. It is suggested that nanosheets process is useful for materials design for nanostructured perovskite oxides with tailored dielectric properties.

4. CONCLUSIONS

Perovskite oxides of $\text{Sr}_{0.5}\text{NbO}_3$ and $\text{Sr}_{0.5}\text{TaO}_3$ and complex perovskite oxides $\text{Sr}_{0.5}\text{Nb}_{0.5}\text{Ta}_{0.5}\text{O}_3$ were successfully obtained via nanosheet process from $(\text{SrNb}_2\text{O}_7)^{2-}$ and/or $(\text{Sr}_{1.5}\text{Ta}_3\text{O}_{10})^{2-}$ nanosheets. AFM images showed that the thickness of $(\text{SrNb}_2\text{O}_7)^{2-}$ and $(\text{Sr}_{1.5}\text{Ta}_3\text{O}_{10})^{2-}$ nanosheets was approximately 6 nm and 4 nm, respectively. XRD and Raman spectra demonstrated that B-site cations in NP- $\text{Sr}_{0.5}\text{Nb}_{0.5}\text{Ta}_{0.5}\text{O}_3$ are arranged to form a superlattice-like structure composed of the layers of $\text{Sr}_{0.5}\text{NbO}_3$ and $\text{Sr}_{0.5}\text{TaO}_3$ along the c axis (B-site-cation ordering), which is different from the randomly distributed B-site cations in SSR- $\text{Sr}_{0.5}\text{Nb}_{0.5}\text{Ta}_{0.5}\text{O}_3$ (B-site-cations disorder). NP-samples exhibited a higher ϵ than SSR-samples for $\text{Sr}_{0.5}\text{NbO}_3$ and $\text{Sr}_{0.5}\text{TaO}_3$. ϵ of NP- $\text{Sr}_{0.5}\text{Nb}_{0.5}\text{Ta}_{0.5}\text{O}_3$ was lower than that of SSR- $\text{Sr}_{0.5}\text{Nb}_{0.5}\text{Ta}_{0.5}\text{O}_3$. It is suggested that the arrangement of B-site cations affects ϵ even if the total composition is exactly the same. Nanosheet process has been demonstrated to be useful for materials design for nanostructured perovskite oxides with tailored dielectric properties.

5. ACKNOWLEDGEMENT

This study was supported by Industrial Technology Research Grand Program in 2006 from New Energy and Industrial Technology Development Organization (NEDO) of Japan.

6. REFERENCES

- [1] M. P. Crosnier-Lopez, F. L. Berre and J. L. Fourquet, *Mater. Chem.*, **11**, 1146-1151 (2001).
- [2] S. Tahara and Y. Sugahara, *Langmuir*, **19**, 9473-9478 (2003).
- [3] K. Domen, J. Yoshimura, T. Sekine, A. Tanaka and T. Onishi, *Catal. Lett.*, **4**, 339-343 (1990).
- [4] Y. Takano, S. Takayanagi, S. Ogura, T. Yamadaya and N. Mori, *Solid State Commun.*, **103**, 215-217 (1997).
- [5] S. N. Ruddlesden and P. Popper, *Acta Crystallogr.*, **10**, 538-539 (1957).
- [6] M. Dion, M. Ganne and M. Tournoux, *Mater. Res. Bull.*, **16**, 1429-1435 (1981).

- [7] B. Aurivillius, *Ark. Kemi*, **1**, 463-480 (1949).
- [8] F. L. Berre, M. P. Crosnier-Lopez and J. L. Fourquet, *Mater. Res. Bull.*, **41**, 825-833 (2006).
- [9] M. Fang, C. H. Kim, T. E. Mallouk, *Chem. Mater.*, **11**, 1519-1525 (1999).
- [10] N. S. P. Bhuvanesh, M. P. Crosnier-Lopez, H. Duroy and J. L. Fourquet, *J. Mater. Chem.*, **10**, 1685-1692 (2000).
- [11] Z. Zhong, W. Ding, W. Hou and Y. Chen, *Chem. Mater.*, **13**, 538-542 (2001).
- [12] R. E. Schaak and T. E. Mallouk, *Chem. Mater.*, **12**, 3427-3434 (2000).
- [13] Y. Ebina, T. Sasaki, M. Harada and M. Watanabe, *Chem. Mater.*, **14**, 4390-4395 (2002).
- [14] R. E. Schaak and T. E. Mallouk, *Chem. Commun.*, **7**, 706-707 (2002).
- [15] R. E. Schaak, *Chem. Mater.*, **12**, 2513-2516 (2000).
- [16] Y. Han and I. Park and J. Choy, *J. Mater. Chem.*, **11**, 1277-1282 (2001).
- [17] F. L. Berre, M. P. Crosnier-Lopez, Y. Lalignant and J. L. Fourquet, *J. Mater. Chem.*, **12**, 258-263 (2002).
- [18] P. J. Ollivier and T. E. Mallouk, *Chem. Mater.*, **10**, 2585-2587 (1998).
- [19] T. Sasaki, Y. Ebina, K. Fukuda, T. Tanaka, M. Harada and M. Watanabe, *Chem. Mater.*, **14**, 3524-3530 (2002)
- [20] In this thickness calculation of the nanosheets, the thicknesses were estimated to be (a sum of thickness of one perovskite layer) \times (number of unit layer and water molecule(s) adsorbed on both surfaces of the nanosheets).

(Received December 27, 2006; Accepted January 24, 2007)